© Universiti Tun Hussein Onn Malaysia Publisher's Office

IJIE

Journal homepage: http://penerbit.uthm.edu.my/ojs/index.php/ijie
ISSN : 2229-838X e-ISSN : 2600-7916

The International Journal of Integrated Engineering

Microstructure and Mechanical Properties of Thermally Treated Cr-Mn-Cu Stainless Steel Welds

Amuda[1], M.O.H.[1], Lawal[1], T. F.[1*], Enumah[1], K.S.[1], Omonua[1], F.S.[1]

[1]Materials Development and Processing Research Group, Department of Metallurgical and Materials Engineering, University of Lagos, 101017

*Corresponding author

DOI: https://doi.org/10.30880/ijie.2020.12.04.015
Received 15 May 2019; Accepted 24 February 2020; Available online 30 April 2020

Abstract: Wrought Cr-Mn-Cu stainless steel is an economical low grade austenitic stainless steel with approximate metallurgical and mechanical properties to the standard Ni-Cr grade. Yet, very little information is available about the weldability of the steel, particularly the influence of heat input and thermal treatment on the microstructure and mechanical properties of the welds of the material. Thus, in the present investigation, the mechanical properties in Cr-Mn-Cu austenitic stainless steel subjected to pre-weld and post weld thermal treatments were characterized relative to microstructural features in the welds. Characterisation of microstructure evolution in the thermally treated welds indicated the development of refined cellular/dendritic structure relative to elongated columnar dendritic microstructure in the as-welded base metal. Specifically, pre-welds exhibited coarse grain morphology in contrast to refined morphology in post thermally treated welds. The contrast in grain morphology in the pre-weld and post weld thermally treated welds was attributed to the differential cooling rates in these different thermal treatment conditions. Hardness value in the thermally treated welds decreases with increasing heat input across the various zones of the weld suggesting the development of equilibrium structure in welds subjected to either pre or post-weld thermal treatment. The highest value was however obtained in post-thermally treated welds. Tensile strength was highest in pre-weld thermally treated coupons at 953 MPa followed by as-welded coupons at 947 MPa and the least in post weld thermally treated coupons at 921 MPa. A major finding from the investigation was that tensile strength decreases with increasing heat input across the process parameters considered irrespective of the thermal treatment conditions. This trend was in concord with trend established in literature.

Keywords: Austenitic stainless steel, mechanical properties, microstructure evolution, pre and post weld thermal treatment, sensitization, tungsten inert gas arc welding, welds grain morphology.

1. Introduction

Austenitic stainless steels (ASSs) belonging to the 300 series contain chromium and nickel as the principal alloying elements and represent near to ¾ market share [1,2]. This dominance on market share is a direct consequence of their superior functional properties such as ductility, formability, drawability, strength, toughness, wear resistance and inter-granular corrosion resistance [3, 4]. As such, they find ready application as structural materials for nuclear reactor coolant piping, valve bodies, vessel internals, chemical and process industries, dairy industries, petrochemical industries, storing and transportation of liquefied natural gas [5]. However, the economic challenges associated with

*Corresponding author: lwltaiwo@gmail.com
2020 UTHM Publisher. All rights reserved.

nickel and the volatility in its supplies generated incentive for the development of lower grades in which the nickel is substituted with other austenite forming or stabilising elements such as Mn, Cu and N [2].

The earlier versions of these lower grade ASSs were developed by introducing and increasing the proportion of manganese to conserve nickel; but these were further strengthened by the inclusion of either nitrogen or copper to enhance austenite stabilization capacity of manganese [6]. Taiwade et al. [7] reported that increasing the proportion of manganese in the stainless steel decreases the solubility limit of chromium in the austenite phase resulting in lower chromium proportion. Therefore, the lower grade alternative to the standard 18Cr-8Ni has lower chromium content with 4% Ni, 6-8% Mn and 0.25% N (S20100, S20200) or 3% Cu (S204300) [6, 2]. These lower grade ASSs are considered for their favourable economics as well as their comparable functional properties. Therefore, they are being deployed as competitive alternatives to the standard 18Cr-8Ni austenitic variety in industries but with less restriction on requirements for corrosion resistance [7]. Such industries include those for architectural/building construction, chemical, electrical machinery/equipment, pharmaceuticals and medicine, transportation, defense and armoury, food and beverages, water supply and household consumables [8, 9]. In most of the listed industries, fusion welding is the prime material integration process with the attendant reduction in service related after-weld properties [5, 10]. Thus, most often, the welds exhibit reduced ductility, tensile and impact properties. In some instances, the corrosion resistance is equally affected [11]. The reduction in as-weld properties is attributable to the phase transformations that accompanied fusion joining arising from the welding heat input [12, 13]. For instance, Kumar and Shahi [5] reported that the microstructure of welds in 18Cr-8Ni grade exhibits smaller dendrite size at lower heat input relative to medium and high heat input. Significant grain coarsening has equally been reported at higher heat input particularly in the heat affected zone (HAZs) of the welds [14]. Further, Amuda et al. [15], Urade and Ambade [16] and Vashishtha et al. [12] reported that microstructure evolution in terms of phase structure, chromium carbide precipitation and grain structure is influenced by the heat input arising from the combination of arc current and electrode traverse speed. Taiwade et al. [7] suggested that controlling the solidification time in resolidified weld of low nickel Cr-Mn ASS may enable the welds exhibits slightly different characteristics. They explained that the time required for initiation of carbide precipitation in low nickel Cr-Mn ASS is shorter and the rate of recovery from the phenomena is comparatively poor relative to the standard 18Cr-8Ni grade. Further, low nickel Ni Cr-Mn ASS is more prone to carbide precipitation for a wider range of temperature with identical heat treatments to the standard grade.

Amuda et al. [11] postulated that controlling the cooling dynamics during resolidification is critical towards minimizing the effect of the welding heat on both the microstructure and post-solidification properties of the weld. Literature identified two thermal treatment frameworks for accomplishing such control. One is pre-weld thermal treatment and the other is post-weld thermal treatment [11, 12, 17]. Whilst Alkali et al. [18] reported that pre-weld thermal treatments could assist in controlling carbide precipitation in the welds due to reduced thermal gradients in the standard ASS, Amuda et al. [11] established that pre-weld thermal treatment is only effective in Cr-Mn-Cu ASS grade at temperatures above 300ºC and that post weld thermal treatment is not effective irrespective of the treatment temperature.

Though, Amuda et al. [11] established that pre-weld thermal treatment can minimize carbide precipitation in Cr-Mn-Cu ASS welds and that post-weld thermal treatment is not effective for the same purpose, the influence of these thermal treatments on mechanical properties of Cr-Mn-Cu ASSs was not considered. Therefore, the present investigation seeks to correlate the microstructure evolution in thermally treated Cr-Mn-Cu ASS welds with the ensuing mechanical properties. This is a follow-up investigation to the work of Amuda et al. [11] towards having a holistic understanding of the influence of thermal treatments on the control of carbide precipitation and mechanical properties in Cr-Mn-Cu ASS welds.

2. Materials and Methods

The 4 mm thick stainless-steel sheet used in the present investigation was sectioned into coupons of dimension 150 mm x 75 mm. The spectra composition of the stainless-steel material obtained from ThermoFisher Scientific's High End Optical Emission Spectrometer presented in Table 1, suggests that the material is a Cr-Mn ASS with copper at 1.12 wt%. The surface of the sectioned samples was pre-cleaned by grit blasting followed by subsequent degreasing via deep agitation in a solution of benzene for 5 minutes to remove adhering dirt and grease.

Table 1 - Chemical composition of stainless-steel sheet

	Elemental Composition (wt.%)									
Materials	Fe	C	Si	Mn	P	S	Cr	Ni	Cu	Trace Elements
Austenitic Stainless-Steel Sheet	72.70	0.07	0.45	10.15	0.05	0.01	14.89	0.34	1.12	Balance

Oxy-acetylene flame in the neutral mode (equal mix of oxygen and acetylene) was used to perform pre-weld thermal treatments on the sectioned coupons at temperatures of 180ºC, 220ºC, 260ºC, 300ºC and 340ºC, respectively for 30 minutes. The sample temperature was acquired using handheld scanning pyrometer. Autogenous full bead weld on coupon was produced on the pre-weld thermally treated coupons afterwards using direct current straight polarity (DCEN) arc torch from Tungsten Inert Gas (TIG) welding machine at varying process parameters. The welding arc was shielded and stabilised using argon gas flowing at a rate 12 l/min. The combination of arc current and electrode traverse speeds in Amuda *et al.* [11] adapted for the present investigation is presented in Table 2.

Table 2 - Matrix of process parameter combination adopted for full bead on plate weld

Weld Coupons (WC)	Arc Current (A)	Travel speed (mm/min)	Arc Voltage (V)	Heat Input (J/mm)
WC 1	50	95	20	302
WC 2	90	177	20	293
WC 3	150	417	20	207

The fusion heat delivered to the coupons was estimated using the relationship specified in Equation (1) where *HI* is the heat input (J/mm), *V* is the potential difference (V) across the terminals, *I* is the arc current (A), *v* is the electrode transverse speed (mm/min.) and η is the efficiency of the TIG welding process (0.48) as reported in Amuda *et al.* [15].

$$HI = \frac{\eta IV}{\upsilon} \tag{1}$$

Preliminary sensitisation analysis of the weld coupons produced with the parameters in Table 2 showed that the coupons produced with the heat input of 293 J/mm exhibited strongly ditched structure relative to those produced at heat input of 207 J/mm and 302 J/mm. As such, it was selected as the control sample for the present study and post-weld thermal treatments was effected on 5 of its coupons in a muffle furnace at constant temperature of 650ºC for varying holding times of 30 min, 60 min., 120 min, 180 min, and 240 min, respectively as presented in Table 3.

Table 3 - Matrix of thermal treatments parameters adopted for pre-weld and post weld treatments adapted from Amuda *et al.* [11]

Welding Coupon	Heat Input (J/mm)		Coupons' Treatment Condition									
			Oxy-acetylene Pre-weld					Annealing Post-weld				
WC 2	293	**Temp.(ºC)**	180	220	260	300	340	650				
		Time (Min)	30					30	60	120	180	240

The as-welded control coupons in addition to the thermally treated coupons were sectioned transverse to welding direction and prepared for microstructural characterization following procedures provided in Amuda *et al.* [11]. In-house purpose-built rectifier conforming to the standard provided in ASTM A262 practice A [19] developed by Amuda *et al.* [15] was adapted to examine precipitation of secondary phases in both the as-welded and thermally treated weld coupons. Prior to microstructural characterisation on CEITI metallurgical microscope, etching of the appropriately polished coupons of the as-received base metal was done in a solution of aqua regia (100 ml HCl + 33 ml HNO_3 + 100 ml C_2H_5OH).

Hardness characteristics of the appropriately polished coupons both of the as-welded and thermally treated coupons were evaluated using a Brinell hardness tester with a load of 1500 kgf until a permanent indentation was achieved. Testing was carried out on the coupons preheated at 260ºC and post-weld thermally treated at 650 ºC for 240 min as they are strongly ditched. The test was repeated thrice and the average value recorded. Brinell reading microscope was applied in measuring the diameter of the indentation whilst the hardness value was obtained from the conversion table. Samples for tensile testing were machined from the weld zone of the coupons. Tensile testing was equally conducted thrice on an Instron machine rated 100 KN at a strain rate of $2 \times 10^{-3}s^{-1}$ at room temperature in accordance with ASTM E8/E8M Standard [20]. Prior to the test, the coupons were sectioned and machined to a gauge diameter of 4 mm, gauge length 30 mm, grip external diameter of 6 mm and grip length of 10 mm . The length of reduced section was 40mm as presented in Figure 1. Similar to hardness characterisation, testing was carried out on coupons preheated at 260ºC and post-weld thermally treated at 650ºC for 240min.

Fig. 1 - Specification for tensile coupons

3. Results and Discussion

3.1 Microstructure of As-received Base Metal

The microstructure of the as-received base metal is shown in Figure 2. The microstructure has been previously characterised by Amuda *et al.* [15] in their earlier published study on Cr-Mn-Cu ASS welds. They described the microstructure of the as-received Cr-Mn-Cu stainless steel base metal as consisting of equiaxed fully austenitic matrix microstructure with some carbides dispersed between and within the austenite grains.

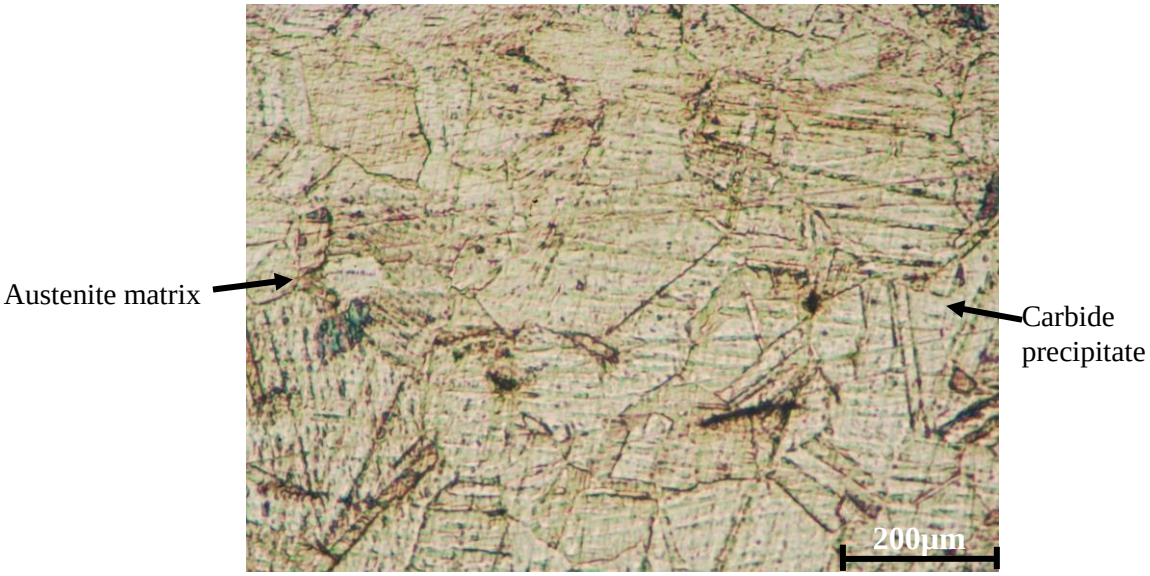

Fig. 2 - Optical micrograph of un-welded, non-thermally treated Cr-Mn-Cu austenitic stainless steel [15]

3.2 Microstructure of Thermally Treated Weld Coupons

Visual observation of the weld tracks revealed absence of defects of any kind. The microstructure of the as-welded Cr-Mn-Cu ASS coupons shown in Figure 3a-c consists of large austenite grains with discontinuous distribution of ferrite phase as discrete islands within the dendritic austenite structure. Amuda *et al.* [15] had reported that the grain morphology in the as-welded coupons is influenced by heat input. The grain structure is elongated in the direction of resolidification with increasing width as the heat input increases. The morphology of the grain structure in the as-welded coupons is considered to be due to the non equilibrium condition of the rapid solidification occurring during fusion welding. This condition allows the peak temperature in fusion zone (FZ) to be much higher than the upper limit of phase balance between δ-fe and γ-fe [14]. This encourages precipitation of austenite at the ferrite grain boundaries during re-solidification of the weld particularly in the welds produced at high heat input. The grain morphologies in the high temperature heat affected zone (HTHAZ) are essentially equiaxed (Figure 4a). Amuda *et al.* [15] attributed the development of such grain structure to the increased fluid flow from increased heat transfer from the center of the weld pool. The dynamics of the grain morphology at the weld interface is influenced by the progression of solidification and cooling rate. Therefore, the morphology consists of a mixture of elongate grains growing into the FZ and equiaxed grains developing towards the HTHAZ. Thus, the weld interface is one with no fixed morphology at any instant until solidification and cooling is complete.

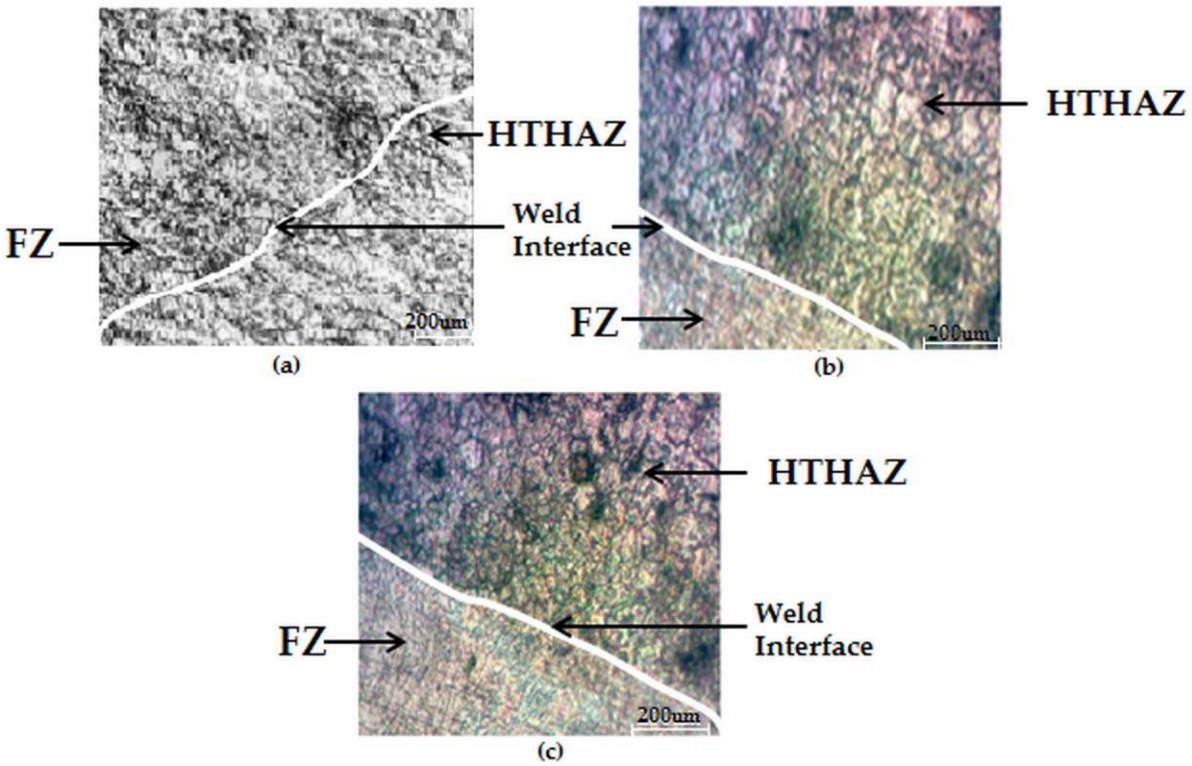

Fig. 3 - Microstructure of as-welded Cr-Mn-Cu ASS at different heat inputs (a) 207 J/mm; (b) 293 J/mm; (c) 302 J/mm

In the pre-weld thermally treated welds, the microstructure is influenced by the characteristics of the thermal gradient in the welds as dictated by the cooling dynamics controlling post solidification structure. Pre-heating with oxy-acetylene changed the behaviour of the thermal gradient from steep gradient to gentle gradient with a slower cooling rate unlike in the as-welded coupons. This permits the resolidified weld to spend greater time above the grain coarsening temperature particularly in the HTHAZ region resulting in coarser grain in the welds (Figure 4b).

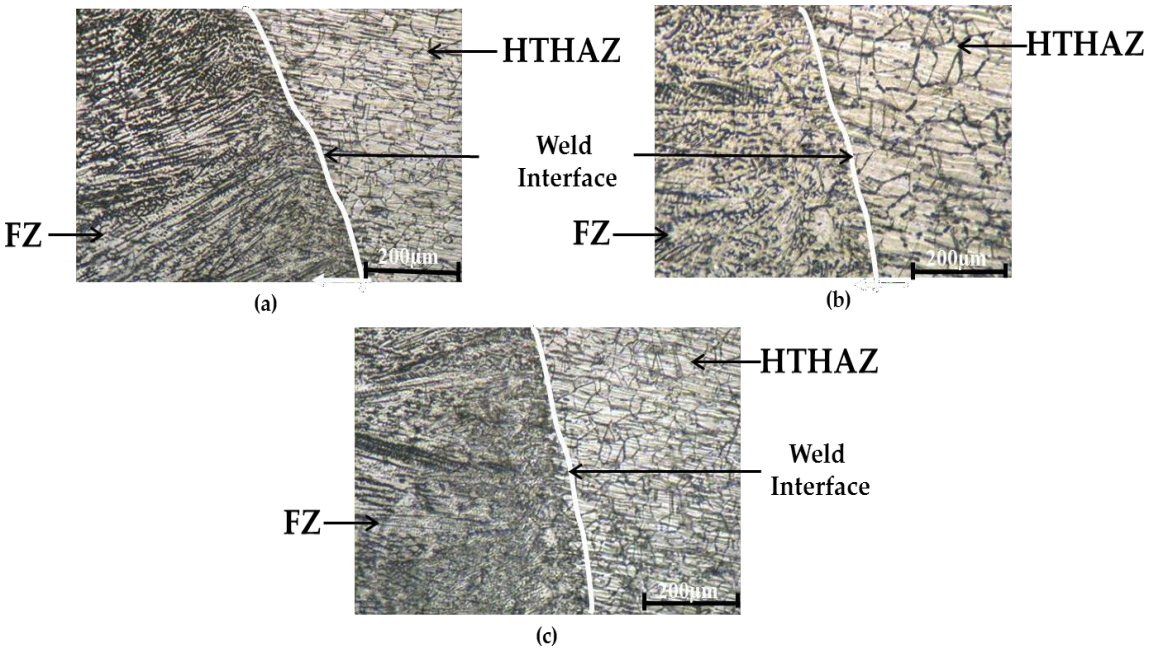

Fig. 4 - Optical micrograph of resolidified weld coupons differential grain morphology (a) As-welded control coupon; (b) Oxy-acetylene pre-weld thermally treated; (c) post-weld thermally treated

Additionally, the gentle gradient condition in pre-weld thermally treated coupons facilitates the development of austenitic/feathery δ-ferrite duplex structure with sparse distribution of ferrite. This implies that pre-weld thermal treatment permits the transformation of δ-ferrite to austenite to proceed in such a way approximating equilibrium cooling condition. Kumar *et al.* [10] had reported similar skeletal ferrite grain morphology and structure in post weld thermally treated 304 ASS welds. This is unlike the morphology obtained in the current investigation in pre-weld thermally treated Cr-Mn-Cu ASS welds. The structure of the grains in post-weld thermally treated coupons reveals further grain growth. However, in contrast to the as-welded coupons, the grain structure in the FZ as well as the HTHAZ of the post-weld thermally treated coupons do not exhibit preferred growth direction (see Figure 4c.).

3.3 Precipitation in Thermally Treated Cr-Mn-Cu Weld Samples

The influence of pre-weld and post weld thermal treatments on carbide precipitation in Cr-Mn-Cu ASS welds as previously reported by Amuda *et al.* [11] revealed that pre-weld thermal treatment is only effective at temperatures above 300ºC as shown in Figure 5a-e. At temperatures below 300ºC, there are deeply ditched structured in the welds which is suggestive of carbide precipitation in the welds. Though, pre-weld thermal treatment at 300ºC and above reveal absence of ditched structure there is increased likelihood of grain coarsening in the welds treated within this temperature range. But in post-weld thermally treated welds, grain coarsening accompanies the inability of the thermal treatment to control carbide precipitation as shown in Figure 6a-c [11].

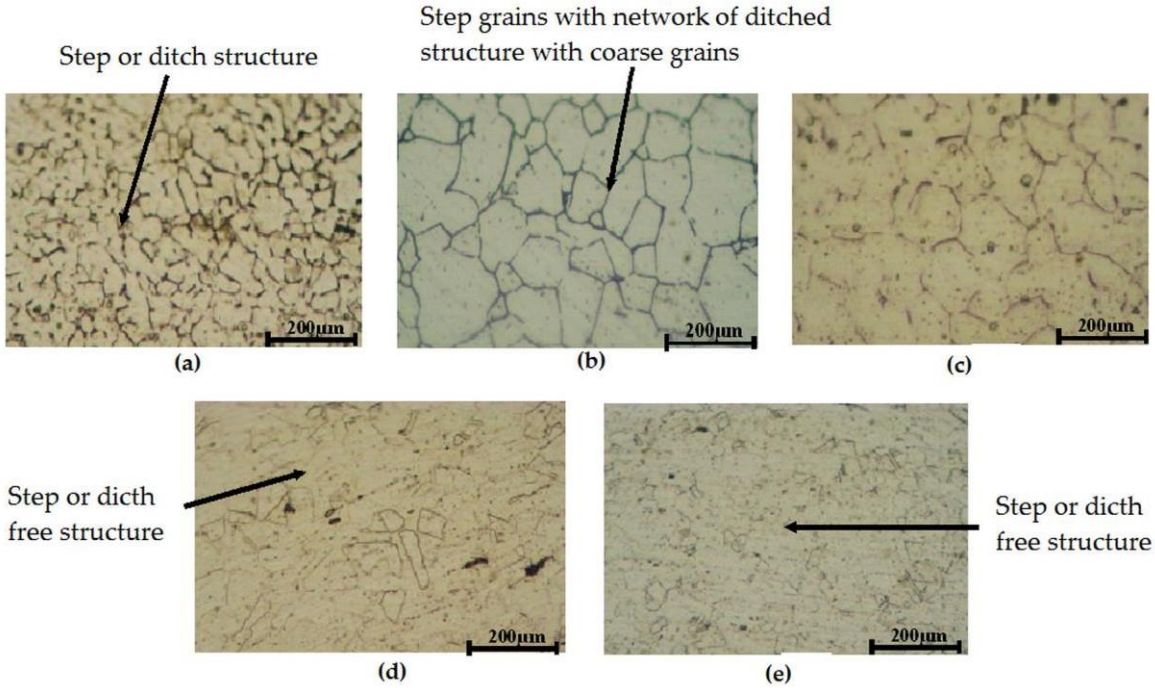

Fig. 5 - Microstructural features within the HTHAZ of welds preheated at different temperatures after 10% oxalic acid etch (a) 180ºC; (b) 220ºC; (c) 260ºC; (d) 300ºC; (e) 340ºC

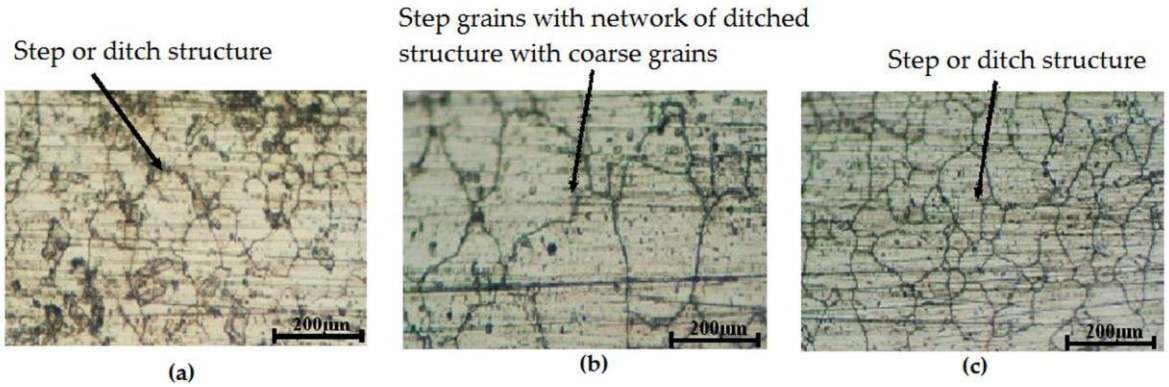

Figure 6 - Microstructural features within the HTHAZ of welds post-weld thermally treated at 650ºC for varying times (a) 30 min; (b) 120 min; (c) 240 min

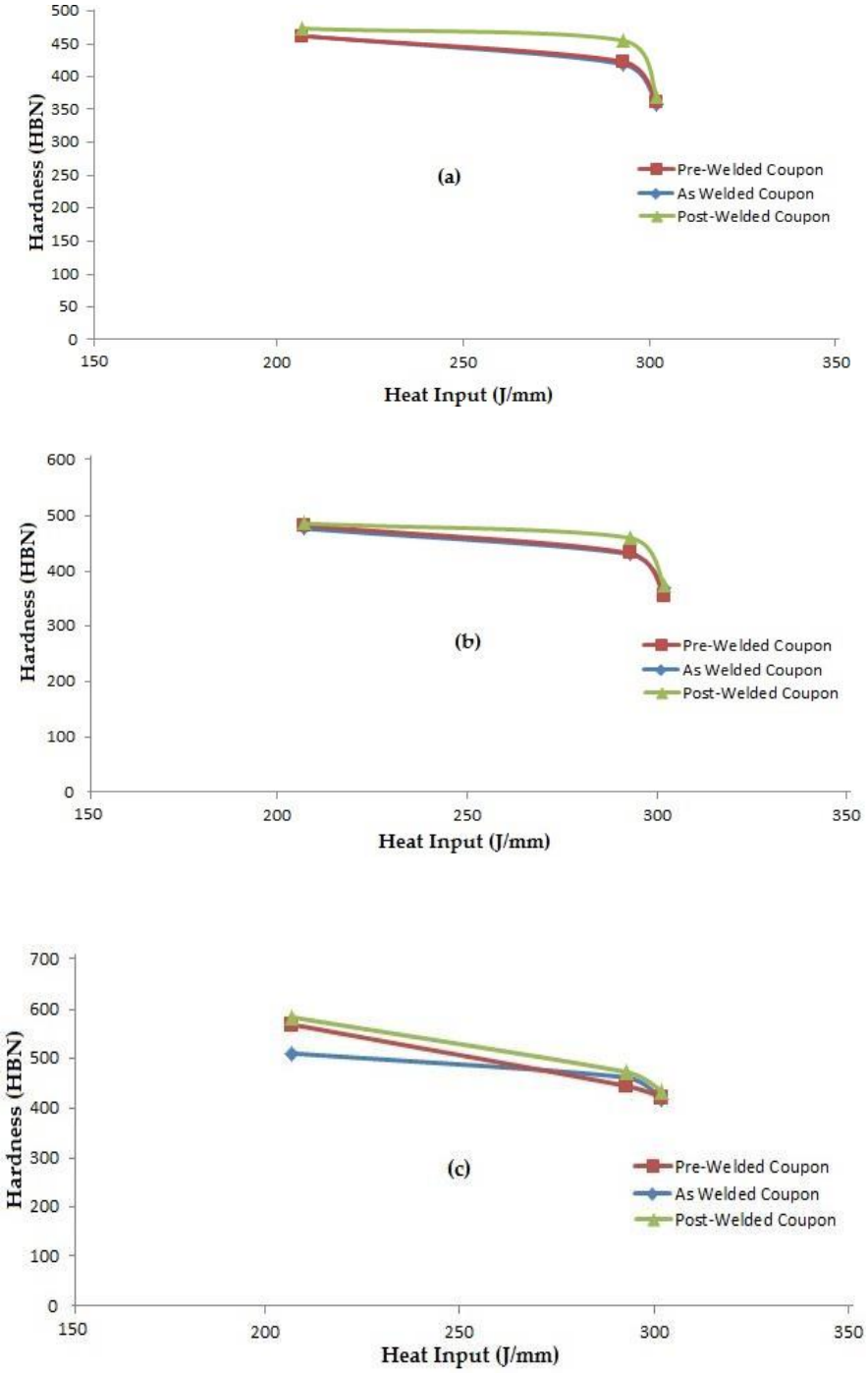

Fig. 7- Hardness characteristics across the various zones in thermally treated Cr-Mn-Cu ASS weld coupons: (a) FZ; (b) HAZ; (c) Base metal

3.4 Analysis of Mechanical Properties

3.4.1 Hardness Analysis in Thermally Treated Welds

The Brinell bulk hardness profile across the weld coupons at different heat inputs in the thermally treated welds is shown in Figure 7. The figure shows that hardness decreases with increasing heat input irrespective of the thermal treatment conditions across the weld major zones of FZ (7a), HAZ (7b) and base metal (7c). Further, as-welded and pre-weld thermally treated coupons exhibit similar hardness characteristics such that it appears that pre-weld thermal treatment has no significant effect on the hardness value in the welds. Post-weld thermal treatment has margina

influence on the hardness value only in the FZ (7a). In other zones of the weld, the hardness trend in post-weld thermally treated coupons is similar to those in both as-welded and pre-weld thermally treated coupons across all heat inputs. But at heat input of 293J/mm the hardness is about 50 point basis higher than those in as-welded and pre-weld thermally treated welds particularly in the FZ. The hardness values in the FZ in the as-welded coupons, pre-weld and post weld thermally treated coupons are 461 HBN, 461 HBN and 472 HBN, respectively at heat input of 207 J/mm. In the HAZ, this value is almost the same (480 HBN) in as-welded, pre-weld and post-weld thermally treated coupons at heat input of 207 J/mm. Beyond this heat input, the hardness progressively decreases until at about heat input of 293 J/mm where the post-weld thermally treated coupons exhibit slightly higher hardness. All the zones show a convergence to lower value of hardness at heat input beyond 293J/mm. The progressive decrease in hardness with increasing heat input could be attributed to grain coarsening accompanying both pre and post-weld thermal treatments. In both thermal treatments, the time spend above the grain coarsening temperature increased due to the transition from steep thermal gradient to moderate thermal gradient resulting in slower cooling rate. The slower cooling rate induced by both pre-weld and post-weld thermal treatments encourages grain coarsening in both the FZ and HAZ as well as the precipitation of chromium carbide in the weld. Ordinarily, such chromium carbide precipitation is expected to pin grain growth at the grain boundary but in the present case, that was not accomplished. The marginal higher hardness value in post-weld thermally treated coupons relative to as-welded and pre-weld thermally treated coupons was attributed to the probable presence of chromium carbide precipitate at the grain boundary which inhibits further grain coarsening as shown in Figure 8. Park *et al.* [21] reported that the formation of Cr-depleted zones in welds arising from slower cooling rate at high heat input may lead to reduction in hardness in such welds.

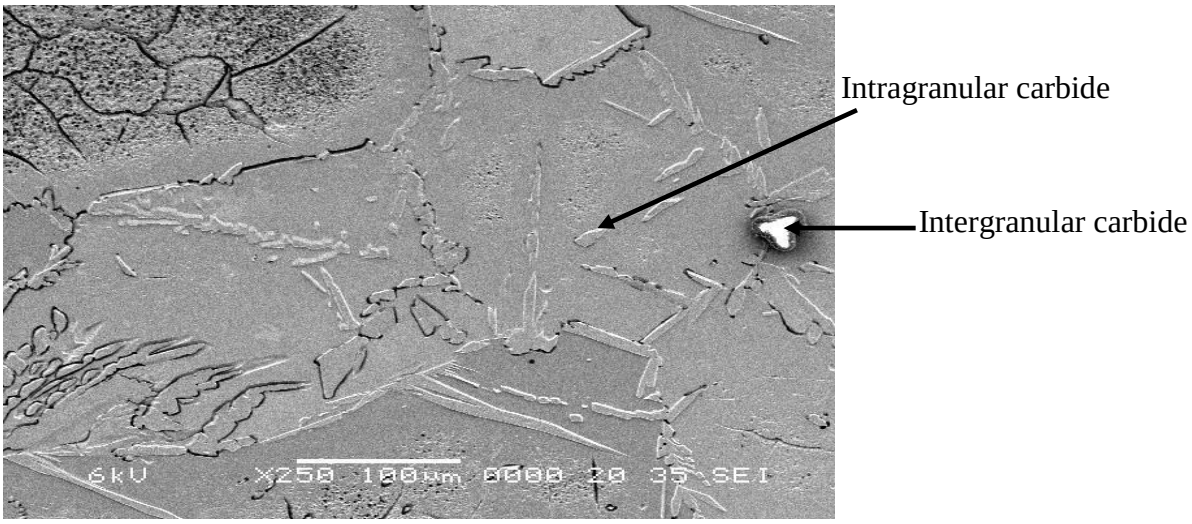

Fig. 8 - Micrograph showing both intragranularly and intergranularly precipitated carbides in coupons post-weld thermally treated at 650ºC

Though, the hardness profiles in the thermally treated welds clearly demonstrate that post-weld thermally treated coupons exhibit the highest hardness across all the heat inputs, but the hardness characteristics across the zones are different. The specific hardness characteristics across the FZ, HAZ and the base metal in coupons post-weld thermally treated at 650ºC presented in Figure 9 show that the base metal exhibits a relatively higher hardness value compared to either the FZ or HAZ. Both the FZ and HAZ present similar hardness profile across the heat inputs. These zones maintained an almost constant hardness of about 500 HBN across the heat inputs until at 293 J/mm beyond which a sharp reduction was observed in hardness value. The base metal on the other hand, exhibits a progressively decreasing hardness value with increasing heat input. The hardness trend in the figure clearly show that the FZ and the HAZ exhibited lower hardness value compared to the base metal. It is believed that the lower hardness obtained in the FZ and HAZ was due to the grain coarsening as well as the depletion of Cr in these regions arising from the heat input. The absence of these phenomena in the base metal is presumed to be due to the restriction of the welding heat within the weld region exclusive of the base metal.

3.4.2 Analysis of Tensile Strength of Thermally Treated Weld Coupons

The tensile strength characteristics against the heat input of the as-welded and thermally treated weld coupons are presented in Figure 10. The figure show that the tensile strength profile exhibit similar reduction trend as obtained in the hardness characteristics in the various thermally treated weld coupons with increased energy input. The figure further demonstrated that the as-welded and then the pre-weld thermally treated coupons exhibit the highest range of

tensile strengths. The maximum tensile energy was achieved at 953 MPa with the pre-weld coupons produced at 203 J/mm while it was 870 MPa when fused at 307 J/mm. The progressive decrease in tensile strength with increasing heat input occurs between 203 J/mm to 293 J/mm. A sharp change was observed in coupons processed above 293 J/mm at which the welds exhibit strengths between 860 MPa to 880 MPa. Thus, it appears that heat input of 293 J/mm represents a threshold of drastic change in the mechanical properties (hardness and tensile strength) of the weld irrespective of thermal treatments. However, while Figure 7 show that post-weld thermally treated coupons exhibit the highest hardness value, the highest tensile strength is obtained in pre-weld thermally treated coupons. The tensile strength in pre-weld thermally treated coupons is 953 MPa. This value is 947 MPa in as-welded coupons whilst in post-

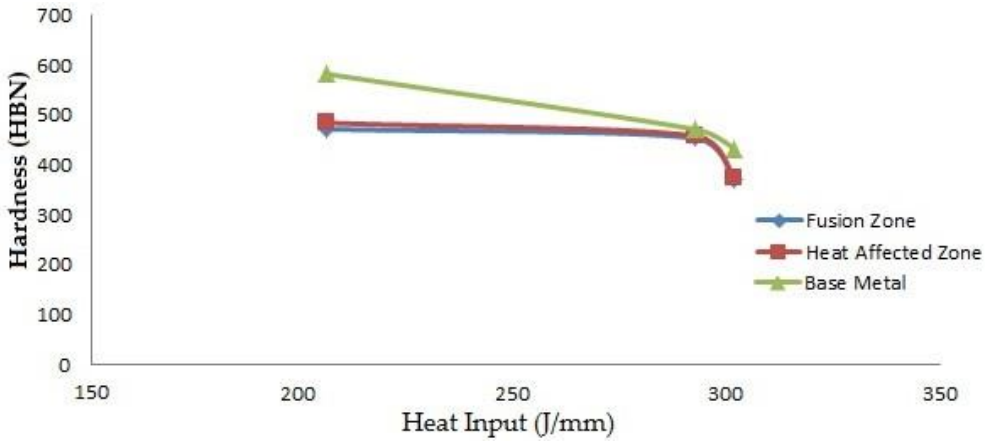

Fig. 9 - The hardness profiles in the thermally treated welds demonstrated that after the post weld thermal processing exhibited the highest hardness across all heat inputs

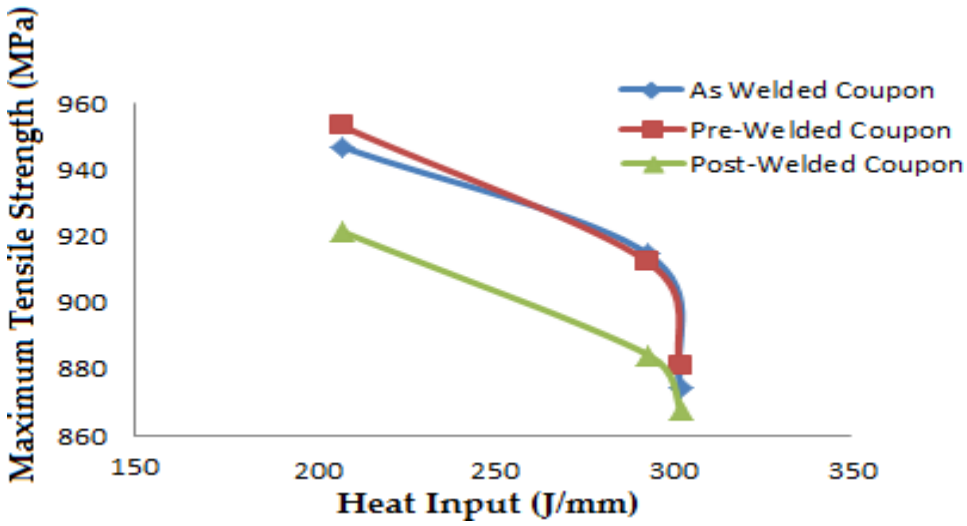

Figure 10 - Tensile strength characteristics in as-welded and thermally treated weld coupons at different heat inputs

weld thermally treated coupons, it is 921 MPa. It is believed that pre-weld thermal treatment enhances carbide precipitation which inhibits movement of dislocation resulting in increasing strength in such welds. Whereas, post-weld thermal treatment though equally enhances carbide precipitation but the rate of grain coarsening is considered higher than the rate of carbide precipitation. Therefore, carbide precipitation cannot keep pace with grain coarsening resulting in lower tensile strength in post-weld thermally treated coupons. Wang *et al.* [22] and Jeon *et al.* [23] reported that the trend in tensile strength variation with changing heat input may equally be explained in terms of dendrites' size as well as the spacing of the dendrites. Increasing heat input induces slower cooling rate which provides sufficient time for dendritic growth, increases inter-dendritic spacing resulting in lower tensile strength [23]. This explains why tensile strength decreases with increasing heat input. Kumar and Shahi [5] reported similar reduction in tensile strength in TIG welded 304 SS and attributed the reduction in strength to dendrite coarsening. This current work corroborates earlier work by Cao [24] and the later work of Damodaram *et al.* [25].

4. Conclusion

The microstructure and mechanical properties of Cr-Mn-Cu ASS welds subjected to pre and post-weld thermal treatments have been characterized. The microstructure of the as-welded Cr-Mn-Cu ASS reveal the presence of large austenite grains with discontinuous distribution of ferrite phase as discrete islands within the dendritic austenite structure. The grain structure is elongated in the direction of resolidification with increasing width as the heat input increases. The morphology consists of a mixture of elongate grains growing into the FZ and equiaxed grains developing towards the HTHAZ. The microstructure in the pre-weld thermally treated welds is influenced by the characteristics of the thermal gradient in the welds as dictated by the cooling dynamics in control of post solidification structure. Pre-heating permits resolidified weld to spend greater time above the grain coarsening temperature particularly in the HTHAZ region resulting in coarser grain in the welds. Additionally, the gentle gradient condition in pre-weld thermally treated coupons facilitates the development of austenitic/ feathery δ-ferrite duplex structure with sparse distribution of ferrite. In post-weld thermally treated coupons, the microstructure evolution reveals substantial grain growth. However, in contrast to the as-welded coupons, the grain structure in the FZ as well as the HTHAZ in the post-weld thermally treated coupons do not exhibit preferred growth direction.

Hardness value in the thermally treated welds decreases with increasing heat input across the various zones of the weld suggesting the development of equilibrium structure in welds subjected to either pre or post-weld thermal treatment. The highest value was however obtained in post-weld thermally treated coupons. The slow cooling associated with post-weld thermal treatment though permits grain coarsening also accelerate carbide precipitation which eventually acts to pin further grain growth. This ultimately results in increased hardness in the welded coupons. Tensile strength was highest in pre-weld thermally treated coupons at 953 MPa followed by as-welded coupons at 947 MPa and the least in post-weld thermally treated coupons at 921 MPa. A major finding from the investigation was that tensile strength decreases with increasing heat input across the process parameters considered. This trend was in agreement trend established in literature.

References

[1] World Stainless Steel Organisation (2016). Stainless steel & its family. *http://www.stainless-steel-world.net/basicfacts/stainless-steel-and-its-families.html*. Accessed on 24 January 2019.

[2] Charles, J., Mithieux, J. D., Santacreu, P. O. & Peguet, L. (2009). The ferritic stainless family: the appropriate answer to nickel volatility?. *Revue de Métallurgie*, 106(3), 124-139.

[3] Feng, Y., Luo, Z., Liu, Z., Li, Y., Luo, Y. & Huang, Y. (2015). Keyhole gas tungsten arc welding of AISI 316L stainless steel. *Materials & Design*, 85, 24-31.

[4] Arivazhagan, N., Singh, S., Prakash, S. & Reddy, G. M. (2011).Investigation on AISI 304 austenitic stainless steel to AISI 4140 low alloy steel dissimilar joints by gas tungsten arc, electron beam and friction welding. *Materials & Design*, 32 (5), 3036–3050.

[5] Kumar, S. & Shahi, A. S. (2011). Effect of heat input on the microstructure and mechanical properties of gas tungsten arc welded AISI 304 stainless steel joints. *Materials & Design*, 32 (6), 3617–3623.

[6] Charles, J., Kosmac, A., Krautschick, J., Simon, J. A., Suutala, N. & Taulavuori, T. (2012). Austenitic chromium–manganese stainless steel–A European Approach. *Materials & Applications*, 12, 1-17.

[7] Taiwade, R. V., Patil, A. P., Patre, S. J. & Dayal, R. K. (2012). A comparative study of intergranular corrosion of AISI 304 stainless steel and chrome-manganese austenitic stainless steel. *ISIJ International*, 52 (10), 1879–1887.

[8] Boniardi, M. V. & Casaroli, A. (2014). Stainless Steels. *Gruppo Lucefin Publishers*, Brescia.

[9] Baddoo, N. R. (2008). Stainless steel in construction: A review of research, applications, challenges and opportunities. *Journal of Constructional Steel Research*, 64 (11), 1199-1206.

[10] Kumar, M., Sharma, A. & Shahi A. S. (2019). A sensitization studies on the metallurgical and corrosion behavior of AISI 304 SS Welds. In: *Advances in Manufacturing Processes. Lecture Notes in Mechanical Engineering.* Springer, Singapore, 257-265

[11] Amuda, M. O. H., Lawal, T. F., Enumah, K. S., Ezeonu, L. L. & Onitiri, M. A. (2018). Influence of thermal treatments on sensitization in Cr-Mn-Cu austenitic stainless steel welds. *UNILAG Journal of Medicine, Science and Technology*, 6(2), 91-106.

[12] Vashishtha, H., Taiwade, R. V, Khatirkar, R. K, Ingle, A. V. & Dayal, R. K. (2014). Welding behaviour of low nickel chrome-manganese stainless steel. *ISIJ international*, 54(6), 1361–1367.

[13] Amuda, M. O. H. & Mridha, S. (2011). Analysis of sensitization profile in medium chromium ferritic stainless steel (FSS) welds. *International Journal of Integrated Engineering*, 3(1), 17-22.

[14] Yan, J., Gao, M. & Zeng, X. (2010). Study on microstructure and mechanical properties of 304 stainless steel joints by TIG, laser and laser-TIG hybrid welding. *Optics & Lasers in Engineering*, 48(4), 512-517.

[15] Amuda, M. O. H., Enumah, K. S., Osoba, L. O. & Onitiri, M. A. (2017). Assessing susceptibility to chromium carbide precipitation in Cr-Mn austenitic stainless steel welds. *UNILAG Journal of Medicine, Science & Technology*, 5(2), 109-122.

[16] Urade, V. P. & Ambade, S. P. (2016). An overview of welded low nickel chrome-manganese austenitic and ferritic stainless steel. *Journal of Material Science & Engineering*, 5(2), 2169-0022.

[17] Mohideen, S. R., & Zaidi, M. A. (2010). Influence of post weld heat treatment on the HAZ of low alloy steel weldments. *International Journal of Integrated Engineering*, 2 (1), 7-11.

[18] Alkali, A. U., Gintar, T. L., Fawad, H. & Abdulrani, A. M. (2014). Influence of preheat flux on the microstructure of 304 stainless steel. *Applied Mechanics & Materials*, 465-466, 1287-1291.

[19] ASTM A 262 (2004). *Standard practises for detecting susceptibility to intergranular attack in austentic stainless steels.* p 1-20, ASTM International, Pennsylvania.

[20] ASTM E8/E8M (2013). *Standard test methods for tension testing of metallic materials*. p 28, ASTM International, Pennsylvania.

[21] Park, S. H. C, Sato, Y. S., Kokawa, H., Okamoto, K., Hirano, S. & Inagaki, M. (2004). Corrosion resistance of friction stir welded 304 stainless steel. *Scripta Materialia*, 51(2), 101–5.

[22] Wang, J., Bai, J., Li, L., Kou, H. & Li, J. (2017). Dendrite size dependence of mechanical properties of in-situ Ti-based bulk metallic glass matrix composites. *Materials Science & Engineering: A*, 704, 77-81.

[23] Jeon, C., Park, J. & Kim, C. P., Kim, H. S. & Lee, S. (2016). Effects of effective dendrite size on dynamic tensile properties of Ti-based amorphous matrix composites. *Metallurgical & Materials Transactions A*, 47(4), 1504–1509.

[24] Cao, X., Rivaux, B., Jahazi, M., Cuddy, J. & Birur, A.(2009). Effect of pre- and post-weld heat treatment on metallurgical and tensile properties of Inconel 718 alloy butt joints welded using 4 kW Nd:YAG laser. *Journal of Material Science*, 44 (17), 4557–4571.

[25] Damodaram, R., Raman, S. G. S. & Rao, K. P. (2014). Effect of post-weld heat treatments on microstructure and mechanical properties of friction welded alloy 718 joints. *Materials & Design*, 53, 954–961.